Improving ionic conductivity by Mg-doping of A2 SnO3 (A = Li+ , Na+)

I. Blazquez-Alcover, G. Rousse, Daniel Alves Dalla Corte, J.C. Badot, A. Grimaud, Patrick Rozier, Jean-marie Tarascon

Improving ionic conductivity by Mg-doping of A_2SnO_3 ($A= Li^+, Na^+$).

I. Blazquez-Alcover [a, d], G. Rousse [a, b, d], D. Alves Dalla Corte [a, d], J. C. Badot [c], A. Grimaud [a, d], P. Rozier[d,e] and J.M. Tarascon [a, b, d, *]

[a] Collège de France, Chaire de Chimie du Solide et de l'Energie, UMR 8260, 11 place Marcelin Berthelot, 75231 Paris CEDEX 05, France

[b] Sorbonne Universités – UPMC Univ Paris 06, 4 place Jussieu, F-75005 Paris, France

[c] Chimie ParisTech, PSL Research University, CNRS, Institut de Recherche de Chimie Paris, 75005 Paris, France

[d] Réseau sur le Stockage Electrochimique de l'Energie (RS2E), FR CNRS 3459 – France

[e] University of Toulouse III Paul Sabatier, CIRIMAT CNRS UMR 5085, 31062, Toulouse Cedex 09, France

*__Corresponding author__: jean-marie.tarascon@college-de-france.fr

Keywords : Ionic conductivity, solid electrolytes, all-solid-state batteries, layered oxides, neutron diffraction.

Abstract.

The search for Li ions conducting ceramics is burgeoning, owing to the regain interest for solid state batteries. Here we investigate the effect of Mg substitutions on the ionic conductivity of the A_2SnO_3 (A = Li, Na) phases. Pure $A_{1.8}Mg_{0.1}SnO_3$ and $A_{2.2}Mg_{0.1}Sn_{0.9}O_3$ were structurally characterized and their ionic conductivity was measured by AC impedance spectroscopy. We show a decrease of the activation energy with increasing the Mg substitution and found ionic conductivities three and two orders of magnitude higher for $Li_{2.2}Mg_{0.1}Sn_{0.9}O_3$ and $Na_{1.8}Mg_{0.1}SnO_3$ as compared to pristine Li_2SnO_3 and Na_2SnO_3, respectively. Neutron diffraction was used to determine the Mg localization in the crystal structure and to provide a rationale for the ionic conductivity changes. Our results confirm the high sensitivity of the ionic conductivity on chemical substitutions, even limited ones.

Introduction.

Liquid electrolyte-based Li-ion batteries are the best candidates to equip electrical devices (vehicles, smart phones…) because of their high energy density.[1,2] However, a major drawback associated to the use of non-aqueous liquid electrolytes is safety, with risks of fires under harsh operating conditions.[3,4] Therefore, constant efforts are being made to replace flammable liquid electrolytes with solid electrolytes, in order to design safer all-solid-state batteries. Research towards Li(Na) based ionic conducting membranes has been intense in the 1980's, but rapidly falls into oblivion because of i) the lack of suitable high ionic conducting materials, ii) the weak rate and cycling capabilities of assembled batteries due to poor interfaces and iii) the high moisture sensitivity of highly conducting sulfides which renders their manipulation difficult without mentioning the possible release of toxic H_2S or SO_2.[5]

Thirty five years have passed and research in solid state batteries is getting back momentum owing to the foreseen interests of the automotive industry. This renaissance has led researchers to revisit the thio-LISICON solid solutions with composition $Li_{4-x}Ge_{1-x}P_xS_4$ (x = 0.75). Recently, Kanno uncovered a new composition with this family with significantly improved Li-ion conduction which is now reaching the values usually achieved for liquid electrolytes at room temperature. This discovery has been made possible by moving towards the tetragonal solid solution with composition $Li_{11-x}M_{2-x}P_{1+x}S_{12}$ (M = Si, Ge, Sn) which displays Li^+ ion conductivities on the order of 10^{-2} $S{\cdot}cm^{-1}$ at room temperature for $Li_{10}GeP_2S_{12}$ and even higher for $Li_{11}Si_2PS_{12}$.[6,7] Taking a different approach, Holtzmann et al. recently reported nearly similar ionic conductivity in the layered sulfide phases $Li_{0.6}[Li_{0.2}Sn_{0.8}S_2]$.[8] These findings provide ionic conductors with high ionic conductivity, but did not address the manipulation issues pertaining to the use of sulfide compounds, neither fully solved the S-Li interface stability. For instance, it was shown that $Li_{4-x}Ge_{1-x}P_xS_4$ degrades into Li_3P, Li_2S and Li-Ge alloy when in contact with Li, hence leading to an increase of the interfacial resistance.[9] Thanks to their greater stability towards Li, oxides could then appear as an alternative to sulfides, hence our search towards Li(Na) ionic conducting oxides besides the LISICON, NASICON, perovskites or garnet families already intensively studied.[10–12]

Interestingly, the phase $Li_{0.6}[Li_{0.2}Sn_{0.8}S_2]$ previously mentioned can simply be viewed as deviating from today's Li-rich layered oxides, the so called Li-rich NMC (ex: $Li_1[Li_{1/3}Ru_{2/3}O_2]$)

that are being presently intensively studied as positive electrodes because of their staggering capacities. The difference simply resides in the facts that we are using i) O rather than S, ii) redox active *d*-metals as opposed to a non-reductive one (Sn is $4d^{10}$) for ensuring minimum electronic conductivity and iii) a full Li^+-containing layer rather than a deficient one. Gladly, the A_2MO_3 (A =Li, Na) family contains other members that are electronic insulator with non-reducing metals such as Li_2TiO_3, Li_2ZrO_3 or $Li_2(Na)_2SnO_3$. In this work, we use the latter compound as our playground to check the feasibility of triggering high ionic conductivity within this type of electronic insulating materials. We tried to enhance its ionic conductivity by playing with the alkaline content via either chemical cationic substitution or reducing conditions to create O vacancies.

Since various attempts to create oxygen vacancies via the reduction of Li_2SnO_3 by CaH_2 or milder reducing agents in sealed ampoules always lead to decomposition into Sn metal, we successfully favor the chemical substitution of either the alkali cation or tetravalent Sn by divalent Mg^{2+} ions to create cationic vacancies or new cationic interstitial sites. The aim of this research will be to compare the conductivity mediated by Li vacancies (A-deficient $A_{2-2x}Mg_xSnO_3$ compounds) and the one given by diffusion through interstitial tetrahedral sites (A-rich $A_{2+2x}Mg_xSn_{1-x}O_3$ compounds). We show that the ionic conductivity of the chemically substituted $A_{2-2x}Mg_xSnO_3$ (x=0.1) and $A_{2+2x}Mg_xSn_{1-x}O_3$ (x= 0.1) with A= Li^+, Na^+ phases increased upon Mg substitution and we explain such an increase in light of the crystallographic sites occupied by the substituent as deduced by neutron studies.

Experimental section.

Synthesis.

Pure A_2SnO_3, $A_{1.8}Mg_{0.1}SnO_3$ and $A_{2+x}Mg_xSn_{1-x}O_3$ phases (x=0.1, A= Li^+ or Na^+) were obtained by classical solid state reaction. Li_2CO_3 (Sigma Aldrich, 99%), Na_2CO_3 (Sigma Aldrich, 99.5%), SnO_2 (Sigma Aldrich, <100nm avg. part. size) and $Mg(OH)_2$ (Sigma Aldrich, 95%) were used as reactants without further purification. Stoichiometric amounts of precursors were weighted with a 10% Li excess in order to compensate for eventual Li loss during the high temperature treatment. In all the cases mixed precursors were ball-milled for one hour and pressed into a pellet subsequently. The different pellets were heated at 950°C in a furnace for 36 hours, with two intermediate grinding in an agate mortar every 12h. Note that attempts to further

dope A_2SnO_3 with Mg were unsuccessful. Doping Mg on the Li site led to the appearance of the double-hexagonal phase $Li_{1.6}Mg_{1.6}Sn_{2.8}O_8$, while doping on the Sn site gave MgO and Li_8SnO_6 as secondary phases.

All the samples were structurally characterized by complementary laboratory, synchrotron X-ray diffraction and neutron powder diffraction prior to be measured for their conductivity measurements.

Characterization.

X-ray diffraction: patterns were first recorded with a Bruker D8 Advance diffractometer equipped with a Cu K_α radiation (λ_1 = 1.54056 Å, λ_2 = 1.54439 Å) and a LynxEye detector to check the purity of the samples. The structural characterization of the different compounds was carefully done by combined neutron and synchrotron X-ray powder diffraction. The synchrotron patterns were collected for A_2SnO_3 and $A_{2.2}Mg_{0.1}Sn_{0.9}O_3$ in a transmission mode (quartz capillary with Ø=0.7mm), with a wavelength of 0.41365 Å at the 11-BM beamline in the Argonne National Laboratory. However, the Na compounds were slightly decomposed because of air exposure and it was not possible to make a reliable fitting. Neutron powder diffraction was carried out for all the samples on the D1B diffractometer at the Institute Laue Langevin with a wavelength of 1.2882 Å and the powder placed in a Ø=5mm vanadium can. All the samples were refined using Rietveld method[13] as implemented in FullProf software.[14]

Attempts to use transmission electronic microscopy to perform localized chemical analysis were not successful because of the phase instability under electron beam.

Ionic conductivity: to carry on the impedance measurements, samples of around 250 mg were pressed into pellets with 10 mm diameter and around 1mm thickness. These pellets were sintered at 950°C for 6 h and cooled down at 1°C/min rate. All the sintered pellets have a real density between 70 and 80 % with respect to the theoretical density of Li_2SnO_3 (4.99 gr/cm^3). Different attempts were made to improve the pellets density by Spark Plasma Sintering (SPS). However, all of these attempts led to phase decomposition by a reduction reaction occurring during the sintering process. Ionic conductivity of the different materials was determined via impedance spectrometry using a MTZ-35 impedance analyzer (Bio-Logic). The measurements were performed using platinum blocking electrodes, in a range of frequencies from 1 MHz to 1 Hz with an applied ac voltage of 500 mV. A thin C foil was placed between the Pt and the pellet

in order to improve the electrode contact. Data were collected in a temperature range from 150°C to 450°C every 25°C.

Structural characterization.

Neutron and synchrotron powder diffraction patterns of Li_2SnO_3 and Na_2SnO_3 were fitted with the space group *C* 2/*c* using the structural model previously reported in the literature. [15,16] Refined lattice parameters are reported in Table 1 and indicate, as expected from the difference in ionic radii, a larger interlayer distance for the Na based compound compared to the Li one. The structure is shown in Fig. 1(a) and consists in stacking of octahedral layers of [AO_6] (A=Li, Na) and 1/3 [AO_6] – 2/3 [SnO_6] layers arranged in a honeycomb pattern. From here, these layers will be referred to as "A layer" or "Sn layer". It is worth to notice the observed differences for the peaks in the 2θ region =[16-22°] for neutrons, [5-6.5°] for synchrotron and related to the Li/Sn ordering in the Sn layers. The broadening observed for these peaks is indicative of the presence of stacking faults, as previously described in the literature. [16,17]

Let us now consider the structure of the Mg doped samples. At a first sight, patterns do not differ much from the stoichiometric pristine ones, indicating that the overall structure is kept. In the Li case, the unit cell increases regularly with the Li amount, but in the Na case, the compound with the greater Na content doesn´t follow the trend (see table 1). Thus, $A_{1.8}Mg_{0.1}SnO_3$ was obtained for both alkaline metals, whereas $A_{2.2}Mg_{0.1}Sn_{0.9}O_3$ was only achieved with Li as we will explain in greater details hereafter.

Table 1. Structural and ionic conductivity parameters (activation energies and extrapolation of the ionic conductivities at room temperature) of Li and Na based compounds.

Li

Composition	Unit cell parameters					Ionic conductivity		
	a (Å)	b (Å)	c (Å)	γ (°)	V (Å^3)	E_a (eV)	σ_{298} (S·cm^{-1})	μ_{298} ($\sigma_{298}\cdot N_{Li}^{-1}V^{-1}$)
$Li_{1.8}Mg_{0.1}SnO_3$	5.291(1)	9.172(3)	10.018(9)	100.19(7)	478.55(1)	0.82	$1.92\cdot10^{-11}$	$2.23\cdot10^{-14}$
Li_2SnO_3	5.298(3)	9.183(4)	10.032(2)	100.23(3)	480.37(8)	0.90	$6.28\cdot10^{-13}$	$6.54\cdot10^{-16}$

$Li_{2.2}Mg_{0.1}Sn_{0.9}O_3$	5.289(8)	9.195(0)	10.061(2)	100.49(4)	481.19(3)	0.76	$2.46 \cdot 10^{-10}$	$2.32 \cdot 10^{-13}$

Na

Composition	Unit cell parameters					Ionic conductivity		
	a (Å)	b (Å)	c (Å)	γ (°)	V (Å^3)	E_a (eV)	σ_{298} (S·cm^{-1})	μ_{298} ($\sigma_{298} \cdot N_{Li}^{-1} V^{-1}$)
$Na_{1.8}Mg_{0.1}SnO_3$	5.504(4)	9.525(2)	11.115(8)	99.49(0)	574.82(1)	0.72	$1.97 \cdot 10^{-11}$	$1.90 \cdot 10^{-14}$
Na_2SnO_3	5.525(7)	9.568(4)	11.085(6)	99.64(1)	577.83(9)	0.83	$2.13 \cdot 10^{-13}$	$1.84 \cdot 10^{-16}$
$Na_{2.2}Mg_{0.1}Sn_{0.9}O_3$	5.511(6)	9.558(4)	11.088(9)	99.74(2)	575.75(7)	0.78	$9.02 \cdot 10^{-13}$	-

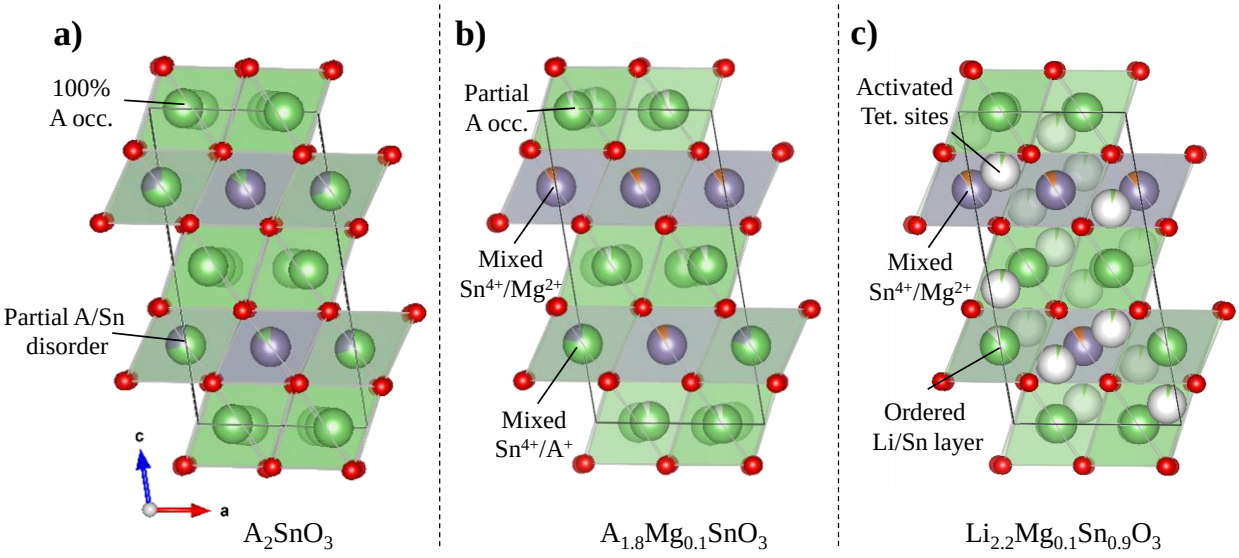

Figure 1. Structural models of a) A_2SnO_3, b) $A_{1.8}Mg_{0.1}SnO_3$ (A=Li, Sn) and c) $Li_{2.2}Mg_{0.1}Sn_{0.9}O_3$. A is green, Sn is purple, O is red and vacancies are white.

Concerning the $A_{1.8}Mg_{0.1}SnO_3$, the structure was further explored to precisely determine the magnesium atomic positions in spite of its low quantity. Different structural models were constructed with magnesium ions sitting i) in the Li positions pertaining to the alkaline or metal layers in emptied octahedral sites, or ii) in the tetrahedral sites present in both layers. The model with Mg^{2+} in the different tetrahedral sites was quickly discarded, since they lead to thermic agitation values out of physical meaning. Calculations for the other two models (octahedral Mg either in Li or metal layer) lead only to slightly different values between the set of B_{iso} and R_{Bragg} parameters. The best fitted model, having the lowest R_{Bragg} and R_{wp} values of 7.6%, 14.7% and 7.0%, 11.2% for Li and Na based compounds, respectively, is presented in Figure 1(b). It consists

of a mixed Sn/Mg and Sn/A metal layer together with a A layer containing the proper amount of cationic vacancies to maintain the material electro neutrality, leading to the overall composition of $A_{1.8}Mg_{0.1}SnO_3$.

Turning to the $A_{2.2}Mg_{0.1}Sn_{0.9}O_3$ compounds, we first note for A=Na the appearance of Bragg peaks associated to MgO impurities (see fig. 2) that we could not eliminate despite of efforts paid on the synthesis conditions (annealing rates, resting temperatures or quench vs. slow cooling temperatures), hence we concluded that pure phase $A_{2.2}Mg_{0.1}Sn_{0.9}O_3$ could not be obtained for Na.

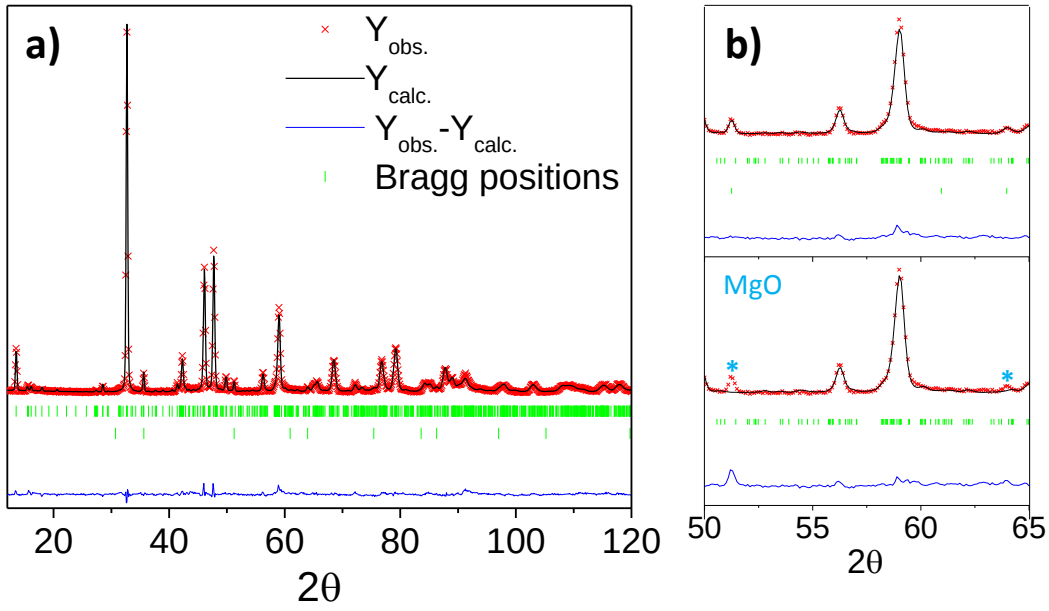

Figure 2. Fitted neutron diffraction pattern of $Na_{2.2}Mg_{0.1}Sn_{0.9}$ (a). Zoom showing the additional peaks before (down) and after (up) add MgO as impurity (b)

In contrast, the compound of nominal composition "$Li_{2.2}Mg_{0.1}Sn_{0.9}O_3$" shows a diffraction pattern alike pristine Li_2SnO_3 and free of extra peaks. Moreover, a more attentive look at this pattern reveals remarkable differences with namely i) some relative intensity changes between the peaks and ii) the sharpening of the superstructure reflections (insets fig. 3) with respect to the pristine and the Li-deficient samples, indicating an absence of stacking faults. In absence of extra phase, the need to maintain the compound electro neutrality implies the partial occupancy of some tetrahedral sites by Li. Assuming that Mg atoms occupy the same metal layer sites as for the Li-deficient compounds; several models were tested to refine the neutron data. The first idea to

come to mind was to place all the extra Li in tetrahedral sites; nevertheless no satisfactory fitting was achieved using this model. The best fit (R_B= 5.25%, R_{wp}= 10.8%) was finally obtained by partially occupying some of the tetrahedral sites but also limiting the occupancy of the Li-metal layer position to 90 %, hence leaving some vacancies in this layer. Therefore, the structure can be written as $Li_{1.5}$(oct.)$Li_{0.25}$(tetr.)[$Li_{0.45}\square_{0.05}Sn_{0.9}Mg_{0.1}$]$O_3$. Figure 1(c) shows the final structural model. Such a migration of Li from octahedral metal layer sites to tetrahedral sites does not come as a total surprise as we have shown that such a migration path can be easily triggered in Li-rich NMC during Li uptake-removal.[18] Moreover, the absence of stacking faults (the pattern shows well defined and sharp superstructure peaks) might also be attributed to the presence of some Li in these tetrahedral sites, as they drive the stacking from one honeycomb LiM_2 layer to another.

Overall, it results from this structural data that the chemical substitution by Mg leads to the creation of alkaline vacancies which are usually viewed as a possible attribute to enhance ionic conductivity.[19]

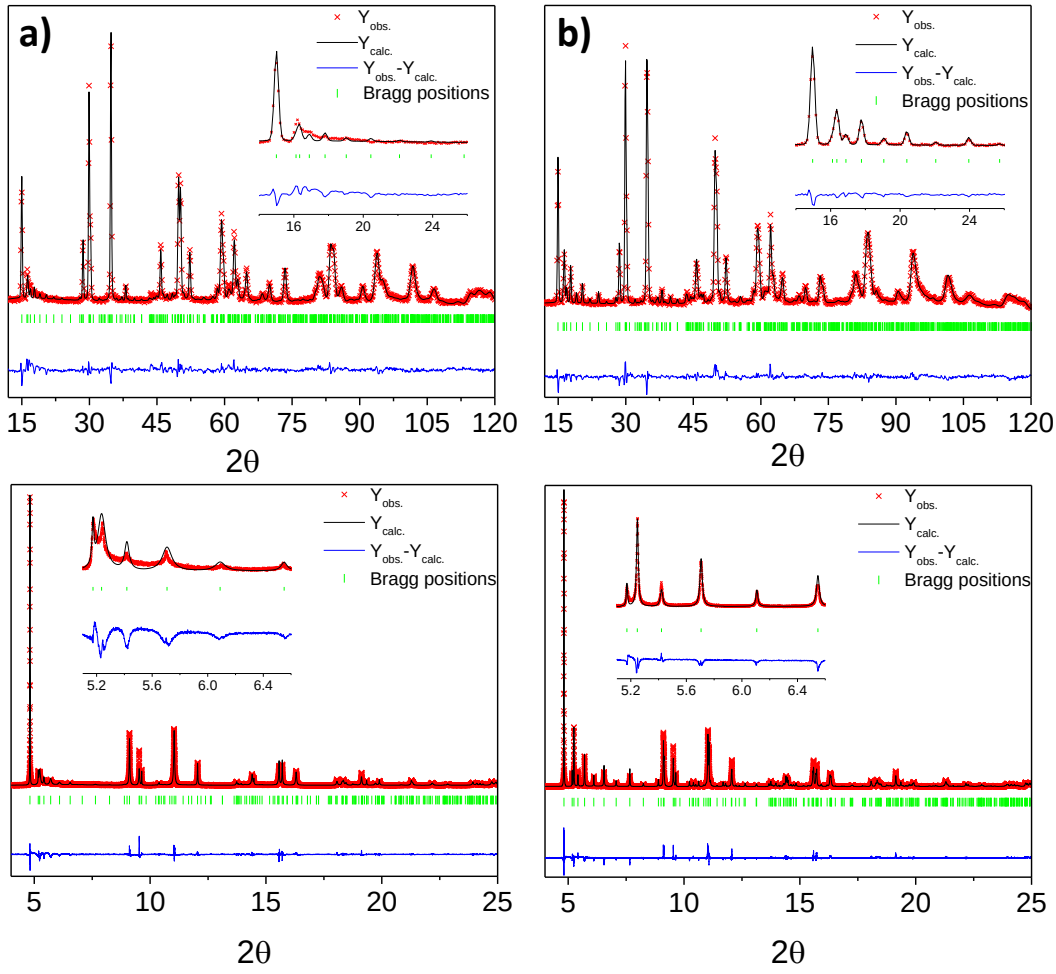

Figure 3. Neutron (up) and synchrotron (down) diffraction patterns and peaks broadening differences (inset) between Li_2SnO_3 (a) and $Li_{2.2}Mg_{0.1}Sn_{0.9}O_3$ (b).

Impedance Spectroscopy.

We measured the ac conductivity for all compounds as a function of temperature till 450°C every 25°C using samples prepared the way described in the experimental section. Figure 4 shows typical Nyquist impedance plots of the sintered pellets at 300°C for the Li (Fig. 4(a)) and Na (Fig. 4(b)) series. The spectra recorded for each members of the series can be described by a depressed semicircle at high-intermediate frequencies (between 10^6 and 10^2 Hz) followed by a low frequency (from 10^2 Hz) spike characteristic of the blocking of mobile Li ions at the electrode interface with Pt blocking electrode. This low-frequency behavior implies that the

sample conductivity is inherently ionic; moreover, DC experiments were carried out for the Li-rich phase and indicated that the electronic contribution to the total conductivity is negligible (see SI). The depression of the semi-circle at high frequency being too high to account for inhomogeneities, it must be decoupled in two different contributions. For clarity, both contributions are shown by two dash semicircles for pristine compounds in Fig 4. These two components can be assigned to the bulk and grain boundary conductivities at high and intermediate frequencies, respectively. The shape of the impedance spectra is preserved in all the range of different temperatures here explored, with therefore a shift to higher frequencies for both bulk and grain boundary contributions. This behavior implies that bulk and grain boundary conductivity can be distinguished in the whole range of temperatures measured.

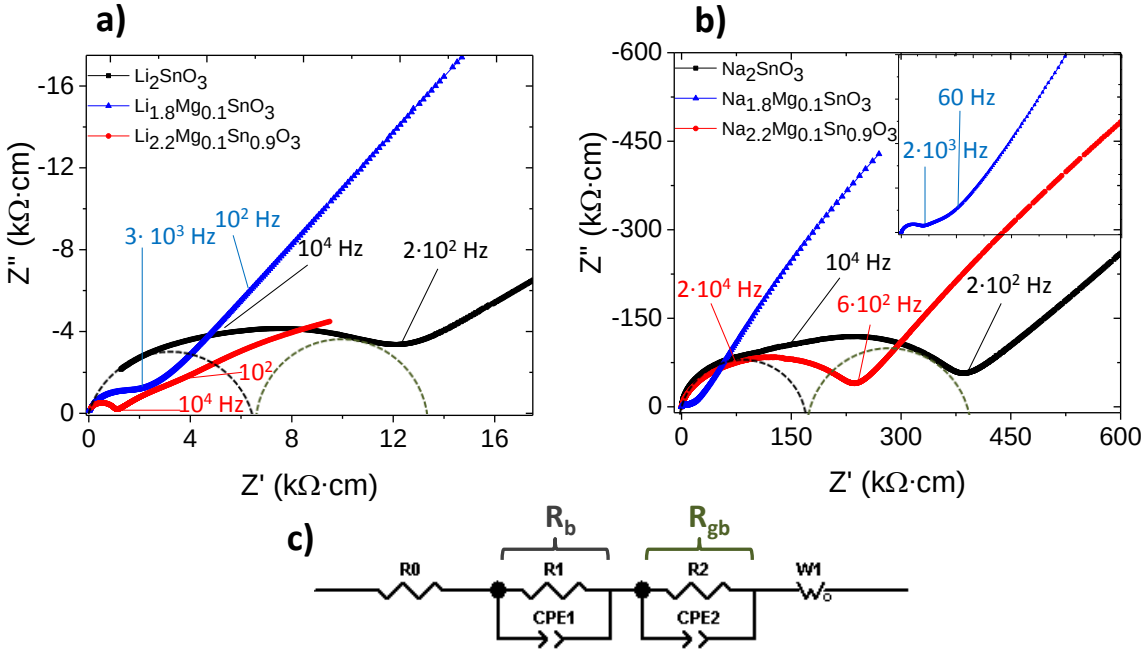

Figure 4. Nyquist plots at 300°C for Li (a) and Na (b) compounds. Pristine compounds are represented in red, A-poor in blue and A-rich in red. Dashed semicircles point bulk (black) and grain boundary (green) conductivities for both pristine compounds. Equivalent circuit used to fit the data (c).

All data were fitted according to the equivalent circuit shown in figure 4(c). Bulk conductivities for each temperature were calculated using the following formula $\sigma_b = d/(S \cdot R_b)$, with d, S and R_b being the thickness, the surface of the pellet and the observed resistance, respectively. The temperature dependence of the bulk conductivity is plotted in Figure 5, showing

an Arrhenius behavior with a linear dependence on 1/T for the bulk ionic conductivity. The activation energies were then extracted from the Arrhenius plots according to the equation:

$$Ln(\sigma \cdot T) = \left(-\frac{E_a}{k_b}\right) \cdot \frac{1}{T} + LnA \ ,$$

where k_b is Boltzmann constant and T the temperature in Kelvin. All activation energies as well as the conductivities at room temperature, obtained by extrapolation, are listed in table 1.

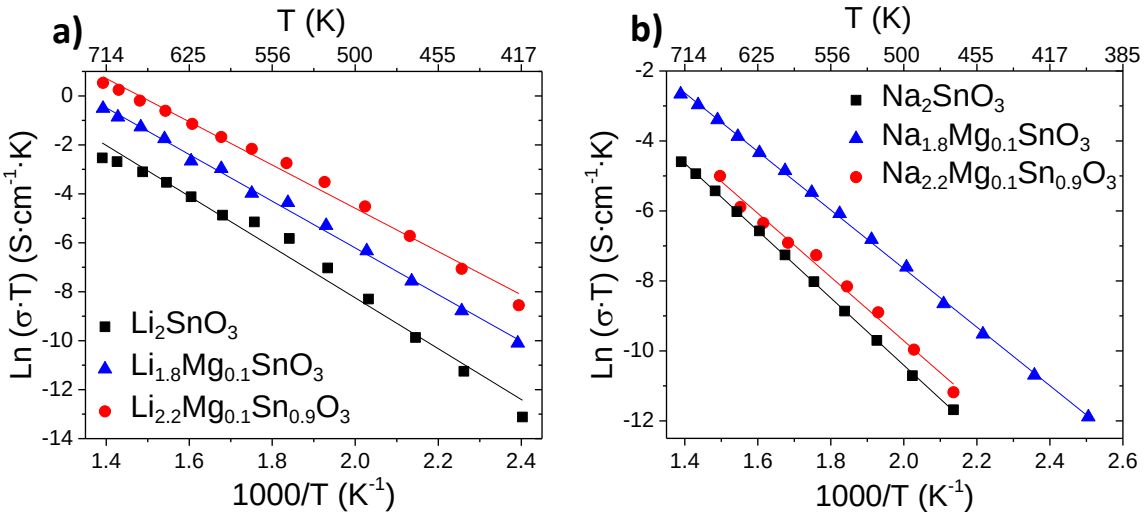

Figure 5. Temperature dependence of ionic conductivity of A_2SnO_3, $A_{1.8}Mg_{0.1}SnO_3$ and $A_{2.2}Mg_{0.1}Sn_{0.9}O_3$ for A= Li^+ (a) and A= Na^+ (b).

For both Li and Na-deficient based compounds we usually observe a two orders of magnitude bulk ionic conductivity increase at room temperature as well as a decrease in the activation energy of nearly ~ 0.1 eV with respect to the pristine. Interestingly, an even larger (three orders of magnitude, from $6.28 \cdot 10^{-13}$ to $2.46 \cdot 10^{-10}$ $S \cdot cm^{-1}$) increase is observed for the Li-rich compound which also shows lower activation energy with respect to the pristine (from 0.90 to 0.76 eV). Lastly, the Na-rich compound does not follow the same trend, as it behaves nearly as the pristine sample. This is not a surprise as we have shown by structural characterization that this phase was not formed.

Assuming the ionic conductivity to follow Nernst-Einstein equation ($\sigma = N \cdot q \cdot \mu$, with N the number, q the charge and μ the mobility of the charge carriers), the difference in conductivity measured for both the Li and the Na solid conductors cannot be explained by the change in charge carriers concentration (from A1.8 to A2.2, with A being Li^+ and Na^+). Based on the structural model previously unraveled, one can tentatively assign the difference in conductivity to structural features. When increasing the amount of Li^+ vacancies going from Li_2SnO_3 to

$Li_{1.8}Mg_{0.1}SnO_3$, the overall conductivity increases by an order of magnitude (Fig. 5a). This enhanced conductivity may demonstrate that alkaline cations diffusion in layered compound can be increased by vacancies-mediated diffusion. Same applies to Na-based layered compounds, going from Na_2SnO_3 to $Na_{1.8}Mg_{0.1}SnO_3$ (Fig. 5b). Moreover, when triggering the partial occupancy of Li+ into tetrahedral position (both in the A and the Sn layers), the overall conductivity is further increased as compared to vacancies-containing compounds (i.e. going from $Li_{1.8}Mg_{0.1}SnO_3$ to $Li_{2.2}Mg_{0.1}Sn_{0.9}O_3$, Fig. 5a). This could indicate that Li+ diffusion mediated by tetrahedral sites would provide lower energy barrier for Li+ to diffuse for layer compounds. Indeed, it is well known that occupying additional interstitial sites can lower the activation barrier for the Li migration in Li-ion conductors.[20] Hence, we believe that even if the octahedral sites are fully occupied, partially occupying the tetrahedral sites may significantly enhance the diffusion in layered compounds in the ab planes. Moreover, considering a 3D diffusion between the different layers, the partial occupation of Li in the octahedral sites of the $Li(Mg/Sn)_2$ layer triggered by the Mg substitution might further enhance the Li diffusion through these planes. Similar examples of ionic conductivity improvement by adding Li^+ in interstitial sites have been recently reported.[21] This observation is in line with, for instance, previous computational work for layered cathode materials where enhanced Li+ diffusion was proposed when triggering a diffusion mechanism through tetrahedral sites.[22,23] Unfortunately, this observation cannot be made for the Na-based layered compounds, since it cannot be synthetized in its over-stoichiometric form. Instead, the conductivity looks alike the stoichiometric Na_2SnO_3 compound, where no vacancies and no tetrahedral sites take part to the diffusion process.

Overall, using the layered A_2SnO_3 family as a model family, some trends can be seen. Even though the ionic conductivity is very limited, we hope that this will bolster further development of layered compounds as ionic conductors, given that the alkaline vacancies-mediated diffusion mechanism as well as the diffusion mediated by tetrahedral sites can be further confirmed for other layered compounds.

Conclusion.

We have reported the partial substitution of either Li(Na) or Sn by Mg into the electronic insulating $Li(Na)_2SnO_3$ phases to successfully produce the Mg-substituted the $Li(Na)_{1.8}Mg_{0.1}SnO_3$ and $Li_{2.2}Mg_{0.1}Sn_{0.9}O_3$ phases. From neutron data, we could deduce that the

Mg atoms are constantly located within the metal layer sites independently of whether we are dealing with Li-deficient or Li-excess phases. Moreover, we show that in both cases the Mg substitution is accompanied by the creation of vacancies located in the Li layer for $Li(Na)_{1.8}Mg_{0.1}SnO_3$ and in the metal layer for the $Li_{2.2}Mg_{0.1}Sn_{0.9}O_3$. Worth mentioning is also the partial occupancy of the tetrahedral sites pertaining to the Li or metal layers to accommodate the extra Li.

Additionally, we show that the Mg-substituted phases have higher ionic conductivities and lower activation energies than the pristine phase with the best values being obtained for the $Li_{2.2}Mg_{0.1}Sn_{0.9}O_3$ which show a room temperature conductivity of $2.46 \cdot 10^{-10}$ $S \cdot cm^{-1}$ and activation energy of 0.7-eV. Needless to say those conductivities are quite too low for these materials to be ever considered as ceramic electrolytes for solid state batteries. Moreover, we experienced that these phases are electrochemically instable against Li and decompose in Sn metallic via conversion reactions for voltages below 1 V.

Fundamental-wise, the ionic conductivity improvement is most likely rooted in the Mg-driven formation of vacancies which act as defects favoring ionic conductivity. Such a simplistic view cannot however explain that the ionic conductivity increase more for the Li-rich as opposed to the Li-deficient phases, while having the same amount of Mg-doping. Although we don't want to over interpret our structural assignment regarding vacancies, we found that they were greater for the $Li_{1.8}Mg_{0.1}SnO_3$ phase, the opposite of what we could have expected. To account for such an explanation, we should recall that the ionic conductivity is defined by $\sigma = ne\mu$ with n being the number of defects and μ is the mobility. So most likely, such defect mobility is at the origin of the greater ionic conductivity observed for the $Li_{2.2}Mg_{0.1}Sn_{0.9}O_3$ phase.

In short, this study further confirms that changes in the mobile ion contents, which lead to the creation of disorder by vacancies or interstitial sites, is an interesting tool to enhance conductivity properties. Therefore, conductivity-wise the Li-rich layered oxides, in contrast to their $Li_{0.6}[Li_{0.2}Sn_{0.8}S_2]$sulfur counter parts, are not the suitable playground for spotting practically viable ionic conductors.

Acknowledgements.

We thank the Réseau sur le Stockage Electrochimique de l'Energie (RS2E) for funding. Use of the 11-BM mail service of the APS at Argonne National Laboratory was supported by the U.S.

Department of Energy under Contract No. DE-AC02-06CH11357 and is greatly acknowledged. We also thank Vivian Nassif for her help in neutron diffraction experiments performed at the D1B diffractometer at the Institut Laue Langevin.

References:

[1] J. Janek, W.G. Zeier, A solid future for battery development, Nat. Energy. 1 (2016) 16141. doi:10.1038/nenergy.2016.141.

[2] D. Larcher, J.-M. Tarascon, Towards greener and more sustainable batteries for electrical energy storage, Nat. Chem. 7 (2014) 19–29. doi:10.1038/nchem.2085.

[3] S. Gallagher, Boeing's Dreamliner batteries "inherently unsafe"—and yours may be too, Ars Tech. (2013). http://arstechnica.com/business/2013/01/boeings-dreamliner-batteries-inherently-unsafe-and-yours-may-be-too/ (accessed November 29, 2016).

[4] Meier, F. & Woodyard, C, Feds review third Tesla fire as shares fall again, USA TODAY. (n.d.). http://www.usatoday.com/story/money/cars/2013/11/07/third-fire-in-tesla-model-s-reported/3465717/ (accessed November 29, 2016).

[5] M. Tatsumisago, M. Nagao, A. Hayashi, Recent development of sulfide solid electrolytes and interfacial modification for all-solid-state rechargeable lithium batteries, J. Asian Ceram. Soc. 1 (2013) 17–25. doi:10.1016/j.jascer.2013.03.005.

[6] N. Kamaya, K. Homma, Y. Yamakawa, M. Hirayama, R. Kanno, M. Yonemura, T. Kamiyama, Y. Kato, S. Hama, K. Kawamoto, A. Mitsui, A lithium superionic conductor, Nat. Mater. 10 (2011) 682–686. doi:10.1038/nmat3066.

[7] S. Hori, M. Kato, K. Suzuki, M. Hirayama, Y. Kato, R. Kanno, Phase Diagram of the Li_4GeS_4-Li_3PS_4 Quasi-Binary System Containing the Superionic Conductor $Li_{10}GeP_2S_{12}$, J. Am. Ceram. Soc. 98 (2015) 3352–3360. doi:10.1111/jace.13694.

[8] T. Holzmann, L.M. Schoop, M.N. Ali, I. Moudrakovski, G. Gregori, J. Maier, R.J. Cava, B.V. Lotsch, $Li_{0.6}[Li_{0.2}Sn_{0.8}S_2]$ – A layered lithium superionic conductor, Energy Env. Sci. (2016). doi:10.1039/C6EE00633G.

[9] S. Wenzel, S. Randau, T. Leichtweiß, D.A. Weber, J. Sann, W.G. Zeier, J. Janek, Direct Observation of the Interfacial Instability of the Fast Ionic Conductor $Li_{10}GeP_2S_{12}$ at the Lithium Metal Anode, Chem. Mater. 28 (2016) 2400–2407. doi:10.1021/acs.chemmater.6b00610.

[10] N. Anantharamulu, K. Koteswara Rao, G. Rambabu, B. Vijaya Kumar, V. Radha, M. Vithal, A wide-ranging review on Nasicon type materials, J. Mater. Sci. 46 (2011) 2821–2837. doi:10.1007/s10853-011-5302-5.

[11] V. Thangadurai, S. Narayanan, D. Pinzaru, Garnet-type solid-state fast Li ion conductors for Li batteries: critical review, Chem. Soc. Rev. 43 (2014) 4714–4727. doi:10.1039/c4cs00020j.

[12] J.C. Bachman, S. Muy, A. Grimaud, H.-H. Chang, N. Pour, S.F. Lux, O. Paschos, F. Maglia, S. Lupart, P. Lamp, L. Giordano, Y. Shao-Horn, Inorganic Solid-State Electrolytes for Lithium Batteries: Mechanisms and Properties Governing Ion Conduction, Chem. Rev. 116 (2016) 140–162. doi:10.1021/acs.chemrev.5b00563.

[13] H. Rietveld, A profile refinement method for nuclear and magnetic structures, J. Appl. Crystallogr. 2 (1969) 65–71.

[14] J. Rodríguez-Carvajal, Recent advances in magnetic structure determination by neutron powder diffraction, Phys. B Condens. Matter. 192 (1993) 55–69.
[15] G. Kreuzburg, F. Stewner, R. Hoppe, Die Kristallstruktur von Li2SnO3, Z. Für Anorg. Allg. Chem. 379 (1971) 242–254.
[16] N.V. Tarakina, T.A. Denisova, L.G. Maksimova, Y.V. Baklanova, A.P. Tyutyunnik, I.F. Berger, V.G. Zubkov, G. Van Tendeloo, Investigation of stacking disorder in Li_2SnO_3, Z. Für Krist. Suppl. 2009 (2009) 375–380. doi:10.1524/zksu.2009.0055.
[17] A. Boulineau, L. Croguennec, C. Delmas, F. Weill, Structure of Li2MnO3 with different degrees of defects, Solid State Ion. 180 (2010) 1652–1659. doi:10.1016/j.ssi.2009.10.020.
[18] M. Sathiya, A.M. Abakumov, D. Foix, G. Rousse, K. Ramesha, M. Saubanère, M.L. Doublet, H. Vezin, C.P. Laisa, A.S. Prakash, D. Gonbeau, G. VanTendeloo, J.-M. Tarascon, Origin of voltage decay in high-capacity layered oxide electrodes, Nat. Mater. 14 (2014) 230–238. doi:10.1038/nmat4137.
[19] R. Chen, W. Qu, X. Guo, L. Li, F. Wu, The pursuit of solid-state electrolytes for lithium batteries: from comprehensive insight to emerging horizons, Mater Horiz. 3 (2016) 487–516. doi:10.1039/C6MH00218H.
[20] T. Asai, S. Kawai, NMR study of Li+-ion diffusion in the solid solution Li3+ x (P1- x, Six) O4> with the γII-Li3PO4 structure, Solid State Ion. 7 (1982) 43–47.
[21] M. Amores, S.A. Corr, E.J. Cussen, Synthesis and Ionic Conductivity Studies of In- and Y-Doped Li6Hf2O7 as Solid-State Electrolyte for All-Solid State Li-Ion Batteries., J. Electrochem. Soc. (2017) A6395–A6400.
[22] Z. Rong, R. Malik, P. Canepa, G. Sai Gautam, M. Liu, A. Jain, K. Persson, G. Ceder, Materials Design Rules for Multivalent Ion Mobility in Intercalation Structures, Chem. Mater. 27 (2015) 6016–6021. doi:10.1021/acs.chemmater.5b02342.
[23] Y. Wang, W.D. Richards, S.P. Ong, L.J. Miara, J.C. Kim, Y. Mo, G. Ceder, Design principles for solid-state lithium superionic conductors, Nat. Mater. 14 (2015) 1026–1031. doi:10.1038/nmat4369.

Supporting Information.

Improving ionic conductivity by Mg-doping of A_2SnO_3 ($A= Li^+, Na^+$).

I. Blazquez-Alcover [a, d], G. Rousse [a, b, d], D. Alves Dalla Corte [a, d], J. C. Badot [c], A. Grimaud [a, d], P. Rozier[d,e] and J.M. Tarascon [a, b, d, *]

[a] Collège de France, Chaire de Chimie du Solide et de l'Energie, UMR 8260, 11 place Marcelin Berthelot, 75231 Paris CEDEX 05, France

[b] Sorbonne Universités – UPMC Univ Paris 06, 4 place Jussieu, F-75005 Paris, France

[c] Chimie ParisTech, PSL Research University, CNRS, Institut de Recherche de Chimie Paris, 75005 Paris, France

[d] Réseau sur le Stockage Electrochimique de l'Energie (RS2E), FR CNRS 3459 – France

[e] University of Toulouse III Paul Sabatier, CIRIMAT CNRS UMR 5085, 31062, Toulouse Cedex 09, France

*__Corresponding author__: jean-marie.tarascon@college-de-france.fr

Keywords : Ionic conductivity, solid electrolytes, all-solid-state batteries, layered oxides, neutron diffraction.

Direct Current measures in $Li_{2.2}Mg_{0.1}Sn_{0.9}O_3$.

To clearly differentiate the electronic conductivity contribution from the total conductivity measured by AC impedance spectroscopy, DC measurements were carried on in the Li-rich $Li_{2.2}Mg_{0.1}Sn_{0.9}O_3$.

DC measurements were done by applying different constant voltages of 0.25, 0.5, 0.75 and 1 V until the current response reached a constant value. The resistance was then calculated averaging the different values got from the steady-state current response using Ohm's law.

Figure S.1. (a) shows the current values collected at different voltages and at different temperatures. In figure S.1. (b) the Arrhenius plot is shown. The electronic conductivity at room temperature was obtained by extrapolation and lead to a value of $2.4 \cdot 10^{-12}$ $S \cdot cm^{-1}$.

The difference between AC and DC measurements is of two orders of magnitude (from 10^{-10} to 10^{-12}) and clearly shows that the contribution of the total (ionic + electronic) conductivity observed by AC impedance is mainly ionic.

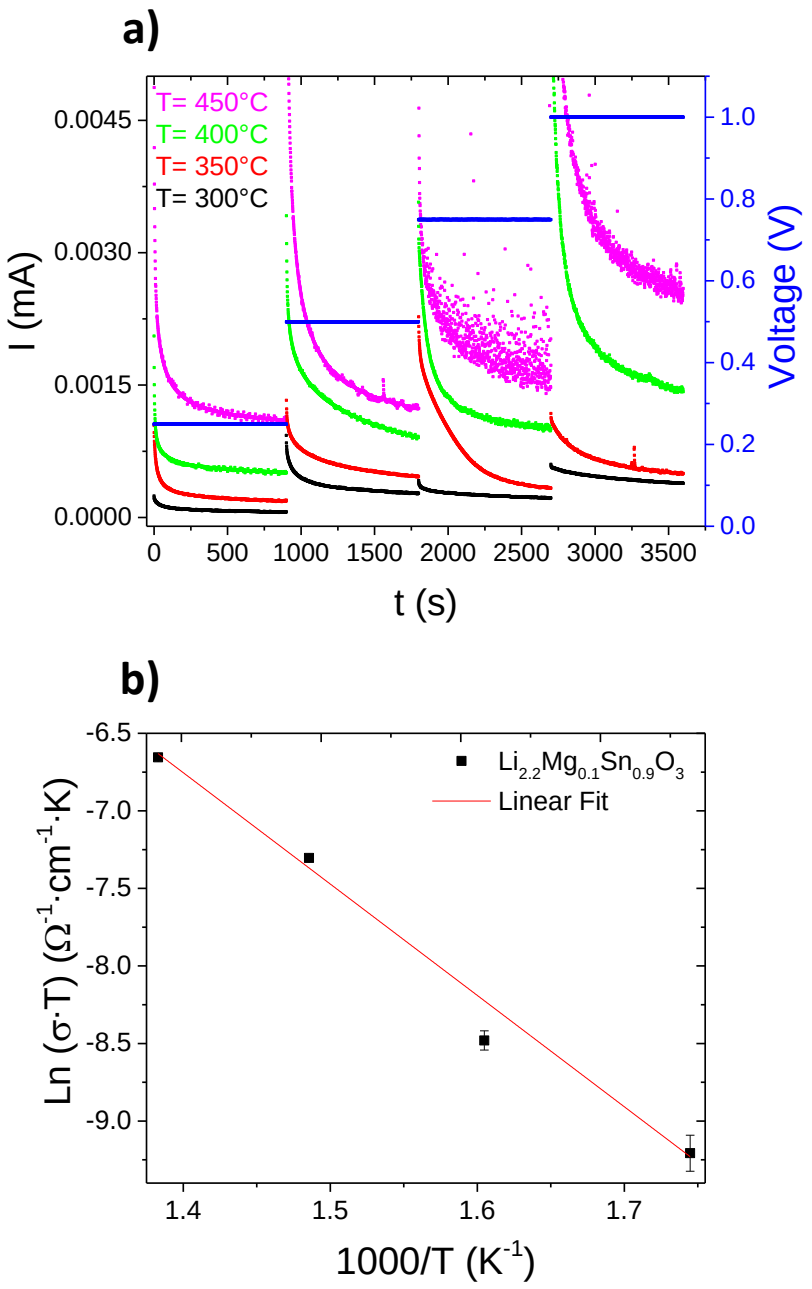

Figure S.1. Chronoamperometry at different potential and temperature for $Li_{2.2}Mg_{0.1}Sn_{0.9}O_3$ (a) and temperature dependence of electronic conductivity (b).